NeuroImage xxx (2013) xxx–xxx

Contents lists available at ScienceDirect

NeuroImage

journal homepage: www.elsevier.com/locate/ynimg

Multimodal imaging of subventricular zone neural stem/progenitor cells in the cuprizone mouse model reveals increased neurogenic potential for the olfactory bulb pathway, but no contribution to remyelination of the corpus callosum ☆

Caroline Guglielmetti [a,1], Jelle Praet [a,b,1], Janaki Raman Rangarajan [c,d], Ruth Vreys [a], Nathalie De Vocht [a,b], Frederik Maes [c,d], Marleen Verhoye [a], Peter Ponsaerts [b], Annemie Van der Linden [a,*]

[a] Bio-Imaging Lab, University of Antwerp, Antwerp, Belgium
[b] Experimental Cell Transplantation Group, Laboratory of Experimental Hematology, Vaccine and Infectious Disease Institute (Vaxinfectio), University of Antwerp, Antwerp, Belgium
[c] Medical Image Computing, ESAT/PSI, Department of Electrical Engineering, & Medical Imaging Research Center, KU Leuven & UZ Leuven, Belgium
[d] iMinds Future Health Department, KU Leuven, Belgium

ARTICLE INFO

Article history:
Accepted 30 July 2013
Available online xxxx

Keywords:
Neural stem cell
Cuprizone
Migration
Remyelination
Magnetic resonance imaging
Bioluminescence imaging

ABSTRACT

Multiple sclerosis is a devastating demyelinating disease of the central nervous system (CNS) in which endogenous remyelination, and thus recovery, often fails. Although the cuprizone mouse model allowed elucidation of many molecular factors governing remyelination, currently very little is known about the spatial origin of the oligodendrocyte progenitor cells that initiate remyelination in this model. Therefore, we here investigated in this model whether subventricular zone (SVZ) neural stem/progenitor cells (NSPCs) contribute to remyelination of the splenium following cuprizone-induced demyelination. Experimentally, from the day of *in situ* NSPC labeling, C57BL/6J mice were fed a 0.2% cuprizone diet during a 4-week period and then left to recover on a normal diet for 8 weeks. Two *in situ* labeling strategies were employed: (i) NSPCs were labeled by intraventricular injection of micron-sized iron oxide particles and then followed up longitudinally by means of magnetic resonance imaging (MRI), and (ii) SVZ NSPCs were transduced with a lentiviral vector encoding the eGFP and Luciferase reporter proteins for longitudinal monitoring by means of *in vivo* bioluminescence imaging (BLI). In contrast to preceding suggestions, no migration of SVZ NSPC towards the demyelinated splenium was observed using both MRI and BLI, and further validated by histological analysis, thereby demonstrating that SVZ NSPCs are unable to contribute directly to remyelination of the splenium in the cuprizone model. Interestingly, using longitudinal BLI analysis and confirmed by histological analysis, an increased migration of SVZ NSPC-derived neuroblasts towards the olfactory bulb was observed following cuprizone treatment, indicative for a potential link between CNS inflammation and increased neurogenesis.

Introduction

Multiple sclerosis (MS) is the most common demyelinating disease of the central nervous system (CNS). Currently, therapeutic interventions are mainly focused on halting or modulating peripheral and CNS immune responses, while only limited research is undertaken towards promoting endogenous repair mechanisms. The latter can be ascribed to the original thoughts that damaged CNS tissue could not be repaired, as neurogenesis was only seen to occur during development. However, due to the discovery of neural stem/progenitor cells (NSPCs) in the adult brain, stimulation of endogenous remyelination processes is emerging as an important therapeutic goal in the treatment of MS (Franklin and Ffrench-Constant, 2008; Menn et al., 2006), as it is well-recognized that endogenous remyelination appears to fail in about 60% of MS lesions (Barkhof et al., 2003). Possible reasons for the latter have most often been studied in animal models for MS. More specifically, the cuprizone mouse model, a toxin-induced murine model for MS without

Abbreviations: AP, antero-posterior; APC/CC1, adenomatous polyposis coli; BG, background; BLI, bioluminescence imaging; CC, corpus callosum; CNS, central nervous system; DV, dorso-ventral; EAE, experimental auto-immune encephalomyelitis; eGFP, enhanced green fluorescent protein; EWD, error weighted difference; fLuc, firefly luciferase; GE, gradient echo; GFAP, glial fibrillary acidic protein; IBA1, ionized calcium binding adaptor molecule; La, lateral; LVv, lentiviral vector; MBP, myelin basic protein; mIPs, minimum intensity projections; MPIO, micron-sized iron oxide particles; MRI, magnetic resonance imaging; MS, multiple sclerosis; NeuN, neuronal nuclear antigen; NSPC, neural stem progenitor cell; OB, olfactory bulb; p75NTR, p75 neurotrophin receptor; p.i., post-injection; PBS, phosphate buffered saline; PC, positive control; PLL, poly-L-lysine; RF, radio-frequency; RMS, rostral migratory stream; ROI, region of interest; sCC, splenium of the corpus callosum; SVZ, subventricular zone; VOI, volume of interest.

* Corresponding author at: Bio-Imaging Lab, University of Antwerp, Campus Drie Eiken (CDE-D.UC.109), Universiteitsplein 1, 2610 Antwerp (Wilrijk), Belgium.
E-mail address: annemie.vanderlinden@ua.ac.be (A. Van der Linden).

[1] Both authors contributed equally to this study.

1053-8119/$ – see front matter © 2013 The Authors. Published by Elsevier Inc. All rights reserved.
http://dx.doi.org/10.1016/j.neuroimage.2013.07.080

the interference of an ongoing auto-immune inflammatory response, is increasingly used to elucidate factors which contribute to de- and remyelination in MS. During the past decade, the sequence of events during de- and remyelination in the cuprizone model, as well as the accompanying molecular and inflammatory events in the CNS, have been characterized extensively (Kipp et al., 2009). In this model, cuprizone treatment induces selective oligodendrocyte apoptosis resulting in demyelination of the CNS main white matter tracts in the corpus callosum (CC), external capsule and striatum. Moreover, demyelination can also be observed in the cortex and hippocampus, albeit at a later timepoint (Skripuletz et al., 2011).

Following acute cuprizone-induced demyelination (*i.e.* 4–6 weeks of cuprizone treatment), remyelination occurs spontaneously. In this context, Petratos et al. (2004) have demonstrated the presence of a subgroup of $NG2^+$ oligodendroglial progenitor cells (OPCs) in the area surrounding the plaques and in the subventricular zone (SVZ) of MS patients. As the same observation was made in the SVZ and in the CC of mice that were treated with cuprizone for 3 weeks, it was suggested that progenitor cells proliferate in the SVZ and subsequently migrate towards the adjacent CC where they differentiate into mature oligodendrocytes (Petratos et al., 2004). Another study by Mason et al. Mason et al. (2000) clearly demonstrated that cell proliferation in the SVZ occurs before the re-appearance of mature oligodendrocytes in the CC. By performing histological analyses at different time points they initially observed the appearance of $NG2^+$ OPCs in the fornix, after which these $NG2^+$ OPCs appeared to migrate into the overlaying CC (Mason et al., 2000). Additionally, increased proliferation of SVZ NSPCs following 3–6 weeks of cuprizone administration has been reported multiple times by means of histological analysis (Chen et al., 2012; Kipp et al., 2009; Mason et al., 2000). Taken together, this suggests an extreme plasticity of the SVZ NSPCs during injury and repair of the CNS.

Current non-invasive imaging modalities for longitudinal tracking of SVZ NSPC migration include magnetic resonance imaging (MRI) and bioluminescence imaging (BLI) (Couillard-Despres and Aigner, 2011; Couillard-Despres et al., 2011; Vande Velde et al., 2012a). For MRI-based cell tracking, numerous studies reported successful *in situ* labeling of SVZ NSPCs following injection of iron oxide particles in the lateral ventricle (Panizzo et al., 2009; Shapiro et al., 2006; Sumner et al., 2009; Vreys et al., 2010) or the SVZ (Nieman et al., 2010). Although only a minor fraction of the injected iron oxide particles becomes internalized by SVZ NSPCs, migration of SVZ NSPC-derived neuroblasts along the rostral migratory stream (RMS) towards the olfactory bulb (OB) could be monitored longitudinally by means of MRI. Moreover, using this technique, a deviation of the steady state RMS migration pathway was demonstrated for SVZ NSPC-derived cells following a hypoxic–ischemic insult (Yang et al., 2009). For BLI-based cell tracking, transduction of the SVZ with a lentiviral vector (LVv) encoding the firefly luciferase (fLuc) reporter protein has been applied successfully to monitor *in vivo* proliferation and migration of SVZ NSPCs towards the OB (Reumers et al., 2008). Given the advantage of longitudinal assessment of *in vivo* SVZ NSPC behavior over single-time point histological analysis, we applied two non-invasive imaging techniques (MRI and BLI) to study the *in vivo* SVZ NSPC behavior and migration following demyelination in the cuprizone model.

Using this experimental approach, we aimed to investigate: (i) whether or not SVZ NSPC contribute to the spontaneous endogenous remyelination of the splenium that occurs in cuprizone model of CNS de/remyelination, and (ii) whether inflammatory and neurode/regenerative processes occurring in the cuprizone model influence the steady state SVZ NSPC-derived neuroblast migration along the RMS towards the OB. In addition, histological analyses are applied to confirm our non-invasive imaging observations at the study end.

Materials and methods

Animals

Female wild type C57BL/6J mice, 8 weeks of age, were obtained *via* Charles River Laboratories (strain code 027) and used for MRI experiments (n = 16). Female C57BL/6J-*Tyr*$^{c\text{-}2J}$/J mice (albino C57BL/6J mice) were obtained *via* Jackson Laboratories (strain code 000058) and further bred in the animal facility of the University of Antwerp. Female offspring of C57BL/6J-*Tyr*$^{c\text{-}2J}$/J mice, 8 weeks of age, were then used for BLI experiments (n = 20). For all experiments, mice were kept in normal day–night cycle (12/12) with *ad libitum* access to food and water. All experimental procedures were approved by the Ethics Committee for Animal Experiments of the University of Antwerp (approval nos. 2006/36 and 2011/13).

Induction of CNS inflammation, demyelination and remyelination

Female C57BL/6J (n = 10) and C57BL/6J-*Tyr*$^{c\text{-}2J}$/J mice (n = 10), 8 weeks of age, had *ad libitum* access to standard rodent lab chow mixed with 0.2% w/w cuprizone (bis(cyclohexanone)oxaldihydrazone, Sigma-Aldrich, Germany) for 4 weeks to induce inflammation and demyelination in the CNS. Following a 4 week 0.2% w/w cuprizone diet, mice were allowed to recover for 8 weeks with *ad libitum* access to standard rodent lab chow. Age matched female control C57BL6 mice (n = 6) and C57BL/6J-*Tyr*$^{c\text{-}2J}$/J mice (n = 10) had *ad libitum* access to standard rodent lab chow during the whole study period.

Preparation of the MPIO–PLL transfection complex

As an MR contrast agent to label SVZ NSPCs, 1.63 μm diameter polystyrene/divinylbenzene-coated fluorescent (Glacial Blue) micron-sized iron oxide particles (MPIOs, 3.00 mg Fe/ml; Bangs Laboratories, Fishers, IN, USA, #ME04F/7833) were used. A cationic polyamine non-viral transfection agent, poly-L-lysine hydrobromide (PLL, MW > 300 kDa, Sigma-Aldrich, Munich, Germany), was used to improve *in situ* cell labeling as previously described (Vreys et al., 2010). Briefly, a PLL stock solution of 1.5 mg/ml was prepared and stored at 5 °C. Prior to injection, the stock solution was further diluted with a 0.9% sodium chloride solution to 0.3 mg/ml and mixed with the MPIOs (3.0 mg Fe/ml), yielding a final MPIO concentration of 0.67 mg Fe/ml with 0.045 mg PLL/ml. MPIO–PLL complexes were placed on a horizontal shaker at 600 rpm for 60 min at room temperature to allow the transfection agent to hybridize with the iron oxide particles. Following preparation, MPIO–PLL complexes were directly used for stereotactic injection.

Lentiviral vector

For genetic labeling of SVZ NSPC we used a previously described LVv encoding both the eGFP and fLuc reporter proteins (LV–eGFP–T2A–fLuc) (Vreys et al., 2010). The LVv was used at a concentration of 2.45×10^8 TU/ml.

Stereotactic injections of MPIO–PLL and LV–eGFP–T2A–fLuc

All surgical interventions were performed according to institutional guidelines. Briefly, mice were anesthetized by intraperitoneal (IP) injection of a ketamine (50 mg/kg for MPIO–PLL injection and 75 mg/kg for LVv injection) (Anesketin; Eurovet NV/SA, Heusden-Zolder, Belgium) + medetomidine (0.65 mg/kg for MPIO–PLL injection and 1 mg/kg for LVv injection) (Domitor; Pfizer Animal Health S.A., Louvain-la-Neuve, Belgium) mixture and positioned in a stereotactic head frame. Stereotactic coordinates to target the right lateral ventricle for MPIO–PLL injection were as follows: AP 1.0 mm, La 0.75 mm and DV 3.3 mm (relative to the bregma). Stereotactic coordinates to target

Please cite this article as: Guglielmetti, C., et al., Multimodal imaging of subventricular zone neural stem/progenitor cells in the cuprizone mouse model reveals increased neurogenic potential ..., NeuroImage (2013), http://dx.doi.org/10.1016/j.neuroimage.2013.07.080

the SVZ of the right lateral ventricle for LVv injections were as follows: AP 1.1 mm, La 1.4 mm and DV 3.0 mm (relative to the bregma), and the needle was then retracted until a depth of 2.3 mm for the second injection. A midline scalp incision was made to expose the skull, and a hole was drilled in the skull using a dental drill burr. Thereafter, an automatic micro-injector pump (kdScientific) with a 10 μl Hamilton syringe was positioned above the exposed dura. A 26-gauge needle (Hamilton) for MPIO–PLL injection or a 32-gauge needle (Hamilton) for LVv injections was attached to the syringe and stereotactically placed through the intact dura and positioned at the respective depth. The needle was left in place for 1 min to allow for pressure equilibration. For MPIO–PLL injection, 2 μl of the MPIO–PLL solution was injected at a speed of 0.5 μl/min. For LVv injection, 2 μl of LVv concentrate was injected at each injection depth at a speed of 0.5 μl/min. Before final needle retraction, a waiting period of 5 min was kept in order to allow for pressure equilibration and to prevent backflow of the injected MPIO–PLL or LVv suspension. Next, the skin was sutured and a 0.9% NaCl solution was given subcutaneously in order to prevent dehydration while mice were placed under a heating lamp to recover. Anesthesia was reversed by an IP injection of atipamezol (Antisedan 5 mg/ml, Pfizer Animal Health S.A.). Immediately following the injection of MPIO–PLL or LV–eGFP–T2A–fLuc, mice were randomly divided into a healthy control group or cuprizone treated group. Cuprizone treatment was initiated immediately following injection.

Bioluminescence imaging, statistics and curve fitting

In vivo BLI was performed according to previously optimized procedures (Reekmans et al., 2011). A total of twenty C57BL/6J-*Tyr*$^{c\text{-}2J}$/J mice, ten which received the cuprizone diet and ten which were fed standard rodent lab chow, were imaged weekly for a period of 12 weeks. Briefly, mice were anesthetized using 2% isoflurane (Isoflo®) in O_2 at a flow rate of 1 l/min. The head of each mouse was shaved before imaging. Mice received an intravenous injection of D-luciferin (150 mg/kg body weight dissolved in PBS; Promega Benelux) and were imaged immediately thereafter for 5 min using an *in vivo* real-time φ-imager system (Biospace). Data was acquired using the Photovision software (v 2.7.5.1) and a photographic image was taken at the end of every acquisition, allowing the BLI signal to be superimposed on this photographic image. For post-processing of BLI measurements, the M3 Vision software (v 1.4) was used. A region of interest (ROI) was manually defined on the photographic image around the OB (0.113 cm^2), the SVZ (0.160 cm^2), the splenium of the CC (sCC, 0.261 cm^2) and a region on the back of the animal located at the level of the two scapulae (0.372 cm^2). This last ROI was considered as background signal and used as internal calibration allowing for comparison between different acquisitions. BLI measurements of these respective ROIs were extracted as photons/s/cm^2/sr and ratios of the BLI signal coming from the OB, SVZ or sCC over the BLI signal coming from the background region were calculated. Results are expressed as mean of the group ± standard deviation for each time point. In order to evaluate the accumulation of labeled cells in the OB over time, data were fitted to a sigmoid model using the NONLIN software package (v 8.00). A two-way repeated measures ANOVA was performed to investigate the time and group differences between the first and the last time point. A paired t-test was also used to investigate the time difference between the first and the last time point within one group. Unpaired t-test was performed to investigate group difference at week 2 p.i. and week 12 p.i. Statistical analysis of the results was performed using SPSS (v 20.0.0) and a p-value < 0.05 was considered to be significant.

Magnetic resonance imaging

MRI was performed at 400 MHz on a 9.4 Tesla MRI system (Biospec 94/20 USR, Bruker Biospin, Germany) using a circular polarized transmit resonator and a quadrature receive surface coil. For *in vivo* MRI experiments, a total of sixteen wt mice, ten which received the cuprizone diet and six which were fed standard rodent lab chow, were used. Anesthesia was induced by inhalation of 3% isoflurane (Isoflo®) and maintained at 1.75% isoflurane in a mixture of 30% O_2 and 70% N_2O at a flow rate of 600 ml/min. Mice were then fixed in an animal restrainer with ear bars and a tooth bar. Throughout image acquisition, respiration rate and body temperature were continuously monitored using a pressure sensitive pad and rectal probe respectively, controlled by the pcSam software interface (SA Instrument Rents, NY, USA). The monitoring system allowed us to maintain the respiration rate at 110 ± 20 breaths/min and the body temperature to 37 ± 0.5 °C. Axial T_2-weighted Fast Spin Echo images were obtained (5 slices, slice thickness = 1 mm, matrix = 256 × 256, FOV = 25 × 25 mm^2, TR = 2500 ms, effective TE = 56 ms, echo train = 8, scanning time = 1 min 20 s). Next, high resolution (isotropic resolution of 78 μm) 3D T_2*-weighted gradient echo (GE) coronal images (matrix = 256 × 196 × 128, FOV = 20 × 15.3 × 10 mm^3 covering the entire brain, TR = 40 ms, TE = 8 ms, 12° flip angle, four repetitions, scanning time = 16 min 43 s per repetition) were acquired. *In vivo* images were acquired after 4 weeks of cuprizone treatment (w4), 4 weeks of cuprizone treatment and 2 weeks of recovery (w4 + 2) or 4 weeks of cuprizone treatment and 8 weeks of recovery (w4 + 8), corresponding to 4, 6, and 12 weeks post-injection of MPIOs into the lateral ventricle.

MR image analysis

The hypo-intense MPIO contrast in MR images was quantified using a semi-automatic image analysis workflow, previously developed for quantification of MRI reporters (Vande Velde et al., 2011, 2012b). First, individual repetitions were registered one-by-one to the first frame and then averaged. A cuboidal volume of interest (VOI) covering the central region of OB in the right hemisphere was once defined on a reference image (template) in Paxinos space (MacKenzie-Graham et al., 2004) and mirrored around the mid-sagittal plane of the template. Subsequently, corresponding bilateral OB VOIs from the right (ipsilateral to MPIO injection,) and left (contralateral to MPIO injection) hemispheres in each of the 3D data sets were automatically delineated by affine registration with the reference template image (Maes et al., 1997). To avoid acquisition related confounding effects like within scan intensity variations all images are first corrected for the RF inhomogeneity induced-bias field using a method as described by Likar et al. (2001). To facilitate comparison of signal intensities between time points and among animals, MR intensities from VOI were normalized to their control region in contra-lateral OB (Meier and Guttmann, 2003). The above-described image analysis steps were fully automated, with identical parameter setting for all images in the given study, which eliminate subjective comparison and ensure reproducible assessment. For qualitative visualization, minimum intensity projections (mIPs) for each 3D data were generated by merging the minimum intensities over 10 sagittal slices, at the level where the RMS enters the OB. These mIPS are free from intensity and position variations, thereby facilitating objective comparison of similar image planes between time points and animals. To visualize altered migration to demyelinated regions, mIPS along coronal section were also created at the level of the splenium of CC (4 slices, anterioposterior coordinates: −1.2 mm up to −1.5 mm, relative to the bregma).

Statistical analysis

For quantitative assessment of MPIO labeled NPSC migration to the OB, intensity histograms from ipsi- and contralateral hemispheres are constructed from intensity normalized MR signal intensities. Using two-sided Mann–Whitney U tests on the histogram values, the contrast difference is statistically assessed (p-value < 0.05). In addition, the bilateral contrast difference is quantified using the error weighted

Please cite this article as: Guglielmetti, C., et al., Multimodal imaging of subventricular zone neural stem/progenitor cells in the cuprizone mouse model reveals increased neurogenic potential ..., NeuroImage (2013), http://dx.doi.org/10.1016/j.neuroimage.2013.07.080

difference (EWD) measure as defined in (Vande Velde et al., 2011, 2012b):

$$EWD = \frac{\mu_{control} - \mu_{test}}{\frac{\sigma_{control}}{\sqrt{N_{control}}}}$$

where, μ, σ and *N* correspond to the mean, standard deviation and the number of voxels of the OB VOI. Positive and large EWD value indicates a strong hypo-intense contrast in the ipsilateral hemisphere, where labeled cells were expected to accumulate. EWD measures from control and experimental groups were compared using a Kruskal–Wallis test. Measures from different time points were compared using a Wilcoxon signed-rank test. A p-value < 0.05 was considered to be significant.

Histological analyses and quantification

Histological analyses were performed according to previously optimized procedures (Praet et al., 2012). Twelve weeks after MPIO–PLL or LVv injection, mice were deeply anesthetized *via* an intraperitoneal injection pentobarbital (60 mg/kg, Nembutal, Ceva Sante Animale) and transcardially perfused with ice cold PBS and perfused-fixed with 4% paraformaldehyde in 0.1 M PBS (pH 7.4). Complete animal heads were post-fixed overnight in 4% paraformaldehyde and whole brains were then surgically removed and freeze-protected by passing through a sucrose gradient (2 h at 5%, 2 h at 10% and overnight at 20%) after which they were frozen in liquid nitrogen and stored at −80 °C until further processing for histological analysis. Consecutive 10 μm-thick cryosections were prepared from the OB, as well as from the front of the injection site until the splenium, using a microm HM500. Slides were screened by direct fluorescence microscopy in order to locate MPIO-containing or eGFP-expressing cells. The number eGFP positive cells in the OB was quantified within a subset of 15 consecutive slices taken in the middle of the OB, by two independent observers, blinded to the experimental groups. Groups were compared using a Mann–Whitney U test with a p-value < 0.05 considered to be significant. Further immunofluorescence analysis was performed using the following antibodies: a rabbit anti-GFAP (Abcam, ab7779, 1/1000 dilution) in combination with a AF555-labeled donkey anti-rabbit secondary antibody (Invitrogen, A31572, 1/1000 dilution), a rabbit anti-IBA1 (Wako, 019-19741, 1/200 dilution) in combination with a AF555-labeled donkey anti-rabbit secondary antibody (Invitrogen, A31572, 1/1000 dilution), a chicken anti-MBP antibody (Millipore, AB9348; 1/200 dilution) in combination with a DyLight549 donkey anti-Chicken secondary antibody (Jackson ImmunoResearch, 703-506-155; 1/1000 dilution), a mouse anti-APC/CC1 antibody (Calbiochem, OP80; 1/200 dilution) in combination with an AF555-labeled goat anti-mouse secondary antibody (Invitrogen, AF21425; 1/300 dilution), a mouse anti-NeuN antibody (Millipore, MAB377; 1/200 dilution) in combination with an AF555-labeled goat anti-mouse secondary antibody (Invitrogen, AF21425; 1/300 dilution). Slides were counterstained using TOPRO-3 (Invitrogen, T3605, 1/200 dilution). Following staining, sections were mounted using Prolong Gold Antifade (Invitrogen, P36930). Fluorescence image acquisition was performed using a standard research fluorescence microscope (Olympus Bx51 fluorescence microscope) equipped with an Olympus DP71 digital camera. Olympus cellSense Software (v 1.4) was used for widefield image acquisition or automated acquisition of optical Z-stacks. Z-stacks were deconvoluted using the cellSense Wiener deconvolution algorithm and a mean intensity projection was made in order to obtain clear single-plane images.

Results

Setup and validation of the cuprizone mouse model

In this study we used the cuprizone model to induce both CNS demyelination and remyelination. In this setup, mice first undergo acute demyelination during 4 weeks of cuprizone intoxication followed by 8 weeks of recovery. In a first experiment, we histologically validated: (i) oligodendrocyte loss and demyelination following 4 weeks of cuprizone treatment, and (ii) the reappearance of oligodendrocytes and remyelination after 8 weeks of recovery. As shown by staining for myelin basic protein (MBP) in Fig. 1, female wt C57BL6/J mice that were on a 0.2% cuprizone diet for 4 weeks (w4) displayed severe demyelination in the splenium as compared to healthy control animals (Control). At this time-point, nuclear TOPRO-3 staining indicated an excessive cell influx (mainly composed of microglia/macrophages, data not shown), while most oligodendrocytes had disappeared, as shown by the absence of staining for $CC1^+$ oligodendrocytes. On a side note, the excessive cell infiltration, combined with edema resulting from the inflammatory reaction, results in a thickening of the splenium at week 4 (the splenium is indicated by the white lines). However, following 8 weeks of recovery (w4 + 8), inflammatory cell accumulation disappeared, as noted by reduced nuclear staining by TOPRO-3. At this time-point, $CC1^+$ oligodendrocytes reappeared and nearly complete endogenous remyelination was observed, as shown by staining for MBP.

MRI analysis of MPIO-labeled SVZ NSPC migration to the OB during de- and remyelination in the cuprizone model

In order to investigate whether SVZ NSPCs display normal migratory behavior during cuprizone-induced de- and remyelination, the following experiment was performed. SVZ NSPCs of the right lateral ventricle were labeled by intraventricular injection of MPIOs. Following MPIO injection, mice were immediately put on a cuprizone-supplemented diet for 4 weeks to induce inflammation and demyelination, followed by 8 weeks of recovery. *In vivo* longitudinal MRI of both healthy control

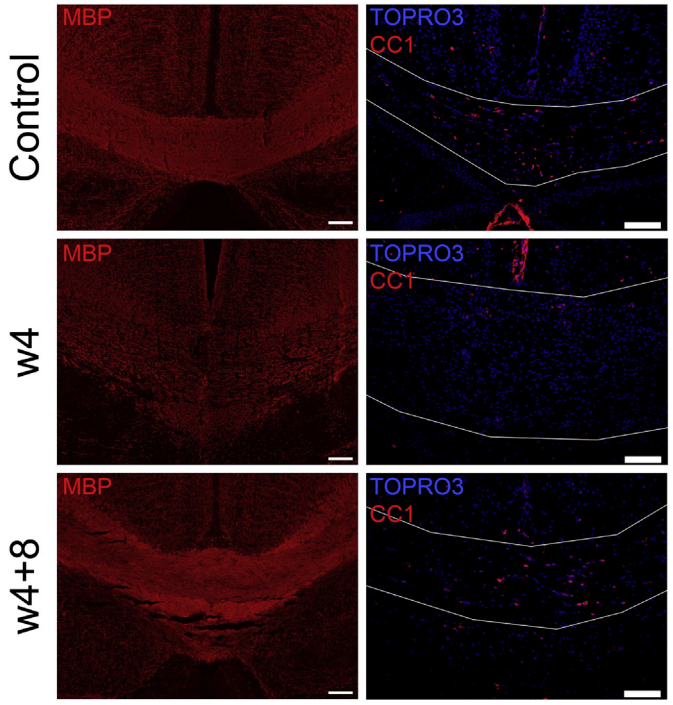

Fig. 1. Setup and validation of the cuprizone mouse model. Representative immunofluorescence images taken at the level of the splenium of the corpus callosum of a control mouse (Control, top row), of a mouse following four weeks on a 0.2% cuprizone diet (w4, middle row) and of a mouse after four weeks on a 0.2% cuprizone diet followed by 8 weeks of recovery on standard rodent chow (w4 + 8, bottom row). The left column shows myelin content by means of staining for myelin basic protein (MBP, red fluorescence). The right column shows $CC1^+$ oligodendrocytes (red fluorescence) and cell density in the CC by means of TOPRO-3 staining (false color, blue fluorescence, scale bar = 50 μm). The splenium is indicated by thin white lines.

Please cite this article as: Guglielmetti, C., et al., Multimodal imaging of subventricular zone neural stem/progenitor cells in the cuprizone mouse model reveals increased neurogenic potential ..., NeuroImage (2013), http://dx.doi.org/10.1016/j.neuroimage.2013.07.080

and cuprizone treated mice was then performed at weeks 4, 6 and 12 after MPIO injection (w4, w4 + 2 and w4 + 8 respectively). The accumulation of MPIO-labeled cells over time in the OB of both the healthy and cuprizone treated mice is visualized on representative minimum intensity projections (mIPs) of T_2*-weighted images as hypo-intense (dark) contrast spots (Fig. 2A, images shown are from 1 representative mouse per group). In both the healthy control group (n = 6) and the cuprizone treated group (n = 10), hypo-intense contrast can be detected along the injection tract, at the level of the ventricles, along the RMS and in the OB of the ipsilateral (right) hemisphere. An accumulation of hypo-intense contrast over time can be visually appreciated in the OB of the ipsilateral hemisphere, however no hypo-intense contrast is observed in the OB of the contralateral hemisphere. Additionally, we quantified the accumulation of MPIO-labeled NSPCs in the OB over time to investigate the effect of cuprizone administration on the constitutive migration of NSPCs from the SVZ towards the OB. VOIs were taken inside the OB in both hemispheres as shown in Fig. 2B, and intensity histograms from these VOIs are shown in Fig. 2C (histograms correspond to the same animal in Fig. 2A). The histograms of the ipsilateral hemisphere OB at each time point for both the control and cuprizone treated groups, showed significant ($p < 0.05$) hypo-intense voxels in the majority of animals (14/16 at w4, 16/16 at w4 + 2 and 14/16 at w4 + 8), reflecting the presence of MPIO-induced hypo-intense contrast within the ipsilateral hemisphere OB. Fig. 2D shows the comparison of EWD measurements over time, and between the cuprizone treated group and the control group. A significant (w4 *vs.* w4 + 8: $p = 0.005$; w6 *vs.* w4 + 8: $p = 0.017$) accumulation of hypo-intense contrast in the ipsilateral OB over time was noted in both groups. However, no difference was detected between the cuprizone-treated group and the control group at any time points (w4: $p = 0.515$; w4 + 2: $p = 0.233$; w4 + 8: $p = 0.386$). In summary, the qualitative and quantitative assessments of MR images suggest that constitutive migration of MPIO-labeled NSPCs from the SVZ towards the OB is not likely impaired during 4 weeks of cuprizone-induced demyelination and subsequent 8 weeks of recovery/remyelination.

Histological validation of MPIO-labeled SVZ NSPC migration to the OB during de- and remyelination in the cuprizone model

Following the above-described results, we histologically validated the uptake of MPIOs by cells in and around the SVZ and their subsequent migration to the OB. Representative IBA1 (microglia), GFAP (astrocytes), NeuN (neurons), and CC1 (oligodendrocytes) immunofluorescence images in Fig. 3A show the SVZ of both the healthy control mice and cuprizone treated mice at week 12 post-MPIO labeling (*i.e.* following 4 weeks of cuprizone treatment and 8 weeks of recovery). No differences were observed between healthy control mice and cuprizone treated mice. Most MPIOs in the SVZ are internalized by $IBA1^+$ microglia, with few MPIOs found to co-localize with $GFAP^+$ cells. Although GFAP is often used as a marker for astrocytes, it is also known to be expressed by SVZ NSPCs (Doetsch et al., 1999). Therefore, it is not unlikely that $MPIO^+$ $GFAP^+$ cells in the SVZ represent, at least partially, MPIO-labeled SVZ NSPCs. Rarely, but not absent, MPIOs were found to co-localize with $NeuN^+$ neurons and $CC1^+$ oligodendrocytes in close

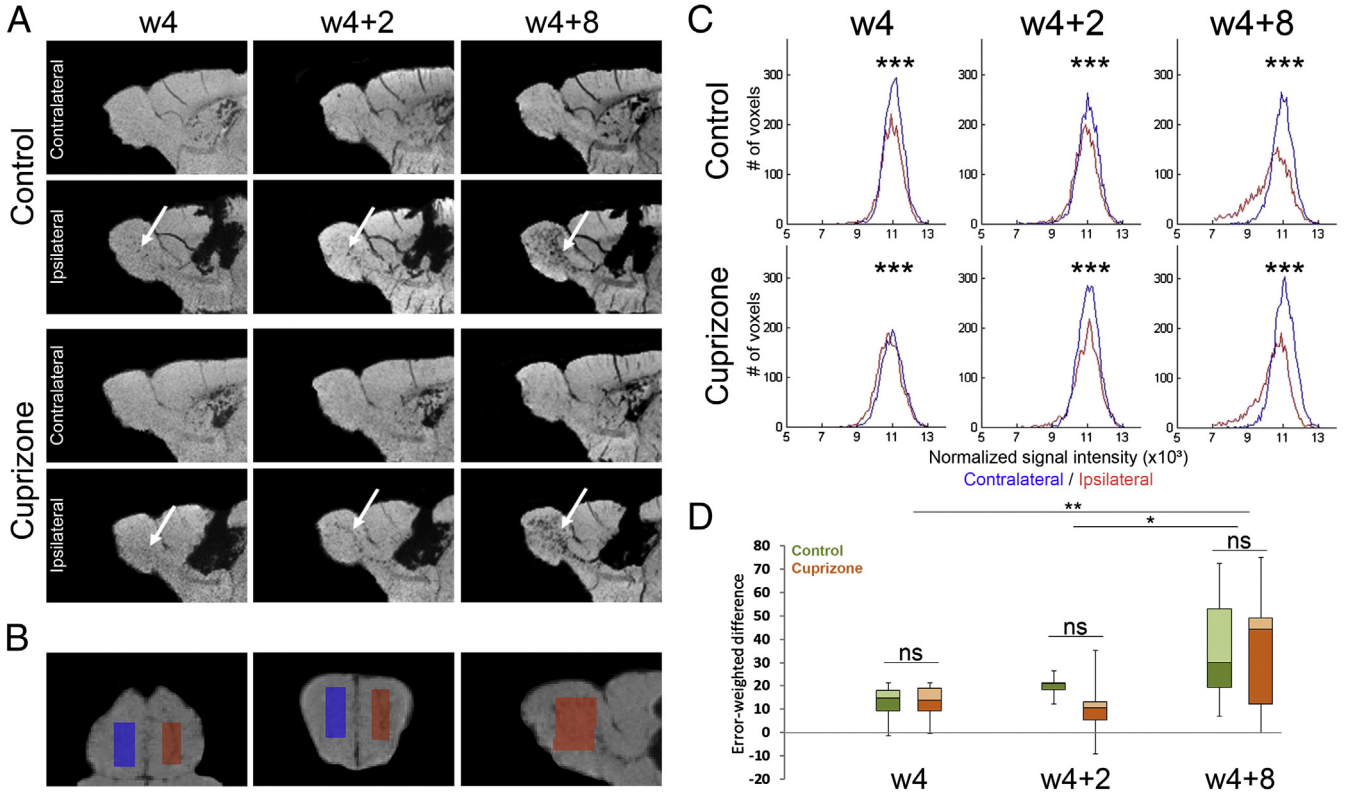

Fig. 2. MRI quantification of MPIO-labeled SVZ NSPC migration towards the OB. (A) Representative sagittal mIPs of 3D gradient-echo MR images acquired *in vivo* at weeks 4, 6 and 12 post-MPIO injection (w4, w4 + 2 and w4 + 8 respectively). Images shown are from a representative age-matched control mouse injected with MPIOs in the lateral ventricle (Control, 2 top rows) and from a representative mouse after a 4-week 0.2% cuprizone treatment followed by 8 weeks of recovery on a regular rodent diet (Cuprizone, 2 bottom rows). Hypo-intense contrast (indicated by the white arrows) in the ipsilateral side of lateral ventricle injection shows migration from the injected area through the RMS and subsequent accumulation over time of MPIOs in the OB. (B) Representative VOIs were automatically generated by our pipeline in the native space of MR images (blue: contralateral OB, red; ipsilateral OB) and used for quantification of hypo-intense voxel load in the OB (left: coronal, middle: axial, right: sagittal planes). (C) Histograms of image intensities extracted from VOIs (blue: contralateral, red: ipsilateral to the MPIO injection) of the corresponding control mouse and cuprizone treated mouse as shown in panel A. Histograms from the contralateral and ipsilateral OB are statistically different and reveal a higher number of hypo-intense voxels in the ipsilateral OB. (D) Boxplots of EWD values per experimental group (green: control group, orange: cuprizone group) and per time point, indicate no difference between both groups at any time points. However, an accumulation of hypo-intense contrast in the ipsilateral OB overtime was noted. (ns: no significance, *: p-value < 0.05, **: p-value < 0.005, ***: p-value < 0.001).

Please cite this article as: Guglielmetti, C., et al., Multimodal imaging of subventricular zone neural stem/progenitor cells in the cuprizone mouse model reveals increased neurogenic potential ..., NeuroImage (2013), http://dx.doi.org/10.1016/j.neuroimage.2013.07.080

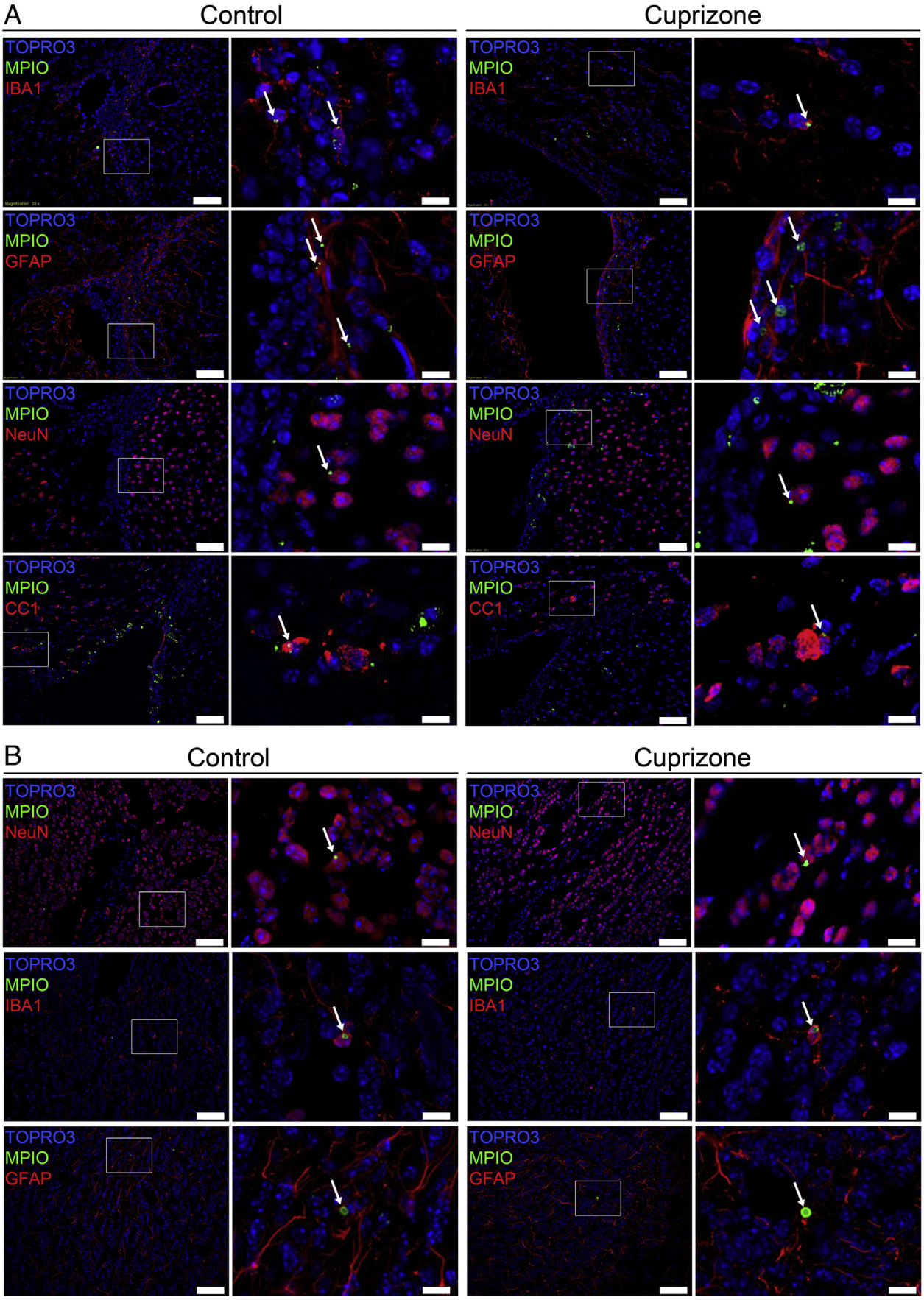

Please cite this article as: Guglielmetti, C., et al., Multimodal imaging of subventricular zone neural stem/progenitor cells in the cuprizone mouse model reveals increased neurogenic potential ..., NeuroImage (2013), http://dx.doi.org/10.1016/j.neuroimage.2013.07.080

proximity to the SVZ or the injection tract. Finally, as shown in Fig. 3B, we also performed immunofluorescence staining for NeuN, IBA1 and GFAP on section from the OB of control and cuprizone-treated mice at week 12 post-MPIO labeling of SVZ NSPC (*i.e.* following 4 weeks of cuprizone treatment and 8 weeks of recovery). Again, no differences were observed between healthy control mice and cuprizone treated mice. While MPIOs were frequently found to co-localize with $NeuN^+$ neurons, thereby confirming the observed migration of SVZ NSPC-derived neuroblasts, MPIOs were also found in $IBA1^+$ microglia and – although to a lesser extent – in $GFAP^+$ cells. Even though further investigation is needed, the latter might indicate that SVZ NSPC migration and differentiation towards the OB is a highly dynamic cell process with multiple cell types or cell stages involved.

MRI reveals no migration of MPIO-labeled SVZ NSPCs towards the demyelinated splenium in the cuprizone mouse model

Within the same experimental setup as described above, we additionally investigated whether SVZ-derived MPIO-labeled NSPCs migrate towards the demyelinated splenium following cuprizone treatment and whether or not they play a role in the renewal of the mature oligodendrocyte pool during remyelination. Visual inspection of T_2-weighted images revealed a hypo-intense (darker) contrast coming from the splenium, characteristic of myelin tissue, in control animals at each measured time point. In contrast, the cuprizone treated group displayed a clear hyper-intense contrast in the splenium after 4 weeks of cuprizone treatment (w4) and after 4 weeks of cuprizone treatment and 2 weeks of recovery (w4 + 2), reflecting demyelination of the splenium and concomitant inflammation (Fig. 4A). However, after 4 weeks of cuprizone treatment and 8 weeks of recovery (w4 + 8), the splenium displayed a similar contrast in the cuprizone-treated group as compared to the control group, which indicates that remyelination had occurred in the cuprizone treated group (Fig. 4A). In addition, axial mIPs created from 3D gradient echo MR images at the level of the splenium were visually inspected and no hypo-intense spots could be detected at w4, w4 + 2 and w4 + 8 post-injection in the cuprizone treated group, suggesting that no migration of SVZ MPIO-labeled NSPCs towards this area had occurred (Fig. 4B). Hypo-intense contrast however could be observed in the ventricles as MPIOs spread along the brain *via* the cerebro-spinal fluid, and as such the latter was not considered to be due to genuine migration of SVZ NSPCs. Fig. 4C shows the histological analysis of both the control and cuprizone treated groups at week 12 post-injection (w12). $MPIO^+$ cells apparently did not migrate into the splenium as no MPIOs could be detected within these regions. MPIOs near the injection tract are shown as a positive control (PC) to illustrate how MPIOs can be identified within the CNS. All together, these results suggest that SVZ-derived NSPCs are most likely not involved in the replenishment of the mature oligodendrocyte pool and the associated remyelination of the splenium.

In situ labeling of SVZ NSPCs with an eGFP–Luciferase encoding LVv confirms the absence of SVZ NSPC migration to the splenium in the cuprizone mouse model

In a complementary experimental setup we used a genetic labeling approach to further characterize/investigate the findings from particle-based NSPC labeling. As we cannot rule out the fact that MPIOs taken up by SVZ NSPCs become diluted upon (potential) high proliferation and differentiation into oligodendrocytes during remyelination in the cuprizone mouse model, we here genetically labeled SVZ NSPCs using a lentiviral vector encoding both the eGFP and Luciferase reporter proteins. The latter allows reproducible tracking of not only the labeled NSPCs themselves, but also their offspring. For this, in albino C57BL/6 mice SVZ NSPCs were *in situ* labeled by injection of an eGFP/fLuc LVv and either: (i) used as control (n = 10), or (ii) subjected to a 0.2% cuprizone diet for 4 weeks starting on the day of LVv injection and left to recover on a normal diet for 8 weeks (n = 10). Mice were imaged weekly during the 12-week observation period in order to monitor SVZ-derived NSPC migration towards the OB and/or the demyelinated splenium. As shown by the representative images at w4, w4 + 2 and w4 + 8 in Fig. 5A, no large BLI signal could be detected caudally to the injection site (*i.e.* the area of the splenium of the sCC), while a distinct BLI signal could be observed in the SVZ and an overtime increasing BLI signal in the OB. In order to quantify putative migration of fLuc-labeled cells from the SVZ towards the sCC, we extracted the BLI signal coming from the background (BG), SVZ and sCC ROIs, as depicted in Fig. 5A, and plotted the ratios of the BLI signal emanating from the SVZ and the sCC, over the background signal (Figs. 5B and C, respectively). The BLI signal in the SVZ remains stable over time for both the healthy control group ($p = 0.7$) or cuprizone-treated group ($p = 0.301$), and no significant differences were noted between the overall BLI signal in the cuprizone-treated group as compared to the healthy control group at week 2 p.i. ($p = 0.077$), nor at week 12 p.i. ($p = 0.071$) (Fig. 5B). The same observation was made in the sCC as the BLI signal remained stable over time for both the control group ($p = 0.199$) and cuprizone treated group ($p = 0.077$). Again, no significant differences were detected between control and cuprizone-treated groups at week 2 p.i. ($p = 0.983$) nor at week 12 p.i. ($p = 0.444$). The latter indicates that fLuc–eGFP labeled cells do not accumulate in the sCC over time (Fig. 5C). Furthermore, it should be noted that: (i) the BLI signal variation over time observed in the sCC is similar to the one observed at SVZ, and (ii) the BLI signal detected in the sCC corresponds to the initial residual value detected in the OB before detection of migrating cells (a ratio OB/background of about 150). Therefore we can conclude that the BLI signal observed in the sCC ROI is likely due to scattered light coming from the transfection area (the SVZ and adjacent parenchyma), as these two ROIs are close in space, and hence no migration of SVZ-derived cells towards the sCC could be detected by means of *in vivo* BLI after *in situ* genetic labeling of SVZ NSPCs. Furthermore, while histological analysis confirmed the presence of eGFP-expressing cells in the SVZ and the surrounding parenchyma, no eGFP-expressing cells were observed in the splenium of the CC at 12 weeks after injection in both the control and cuprizone-treated groups (Fig. 6A), thereby confirming the absence of cell migration from the SVZ to the sCC during remyelination in the cuprizone mouse model.

In situ labeling of SVZ NSPCs with an eGFP–Luciferase encoding LVv reveals increased migration of SVZ NSPC towards the OB in the cuprizone mouse model

Although analysis of SVZ NSPC-derived neuroblast migration towards the OB was originally included as a control to confirm efficient LVv-mediated transduction of SVZ NSPCs (Fig. 5A), we noted significant differences between control and cuprizone-treated mice. In order to quantify migration of fLuc-labeled cells from the SVZ towards the OB, we extracted the BLI signal coming from the OB ROI, as depicted in Fig. 5A, and plotted the ratio of the BLI signal emanating from the OB over the background signal (Fig. 5D). Effective migration of fLuc labeled cells towards the OB can be appreciated by the sigmoidal distribution of the BLI signal over time for both the control and cuprizone groups

Fig. 3. Histological validation of MPIO-labeled SVZ NSPC migration to the OB. Representative immunofluorescence images taken at the site of MPIO injection (A) or in the OB (B), for both healthy control animals (Control) and mice that received a 0.2% cuprizone diet for 4 weeks followed by 8 weeks of recovery on standard rodent chow (Cuprizone). The left picture each time shows a general overview of the injection spot at a low magnification (scale bar = 50 μm), while the area inside the white rectangle is then shown at a higher magnification in the right picture (scale bar = 10 μm). Cell nuclei were stained using TOPRO-3 and are shown in blue (false color), MPIOs are shown in green (false color) and the corresponding markers (IBA1, GFAP, NeuN and CC1) are shown in red (red fluorescence).

Please cite this article as: Guglielmetti, C., et al., Multimodal imaging of subventricular zone neural stem/progenitor cells in the cuprizone mouse model reveals increased neurogenic potential ..., NeuroImage (2013), http://dx.doi.org/10.1016/j.neuroimage.2013.07.080

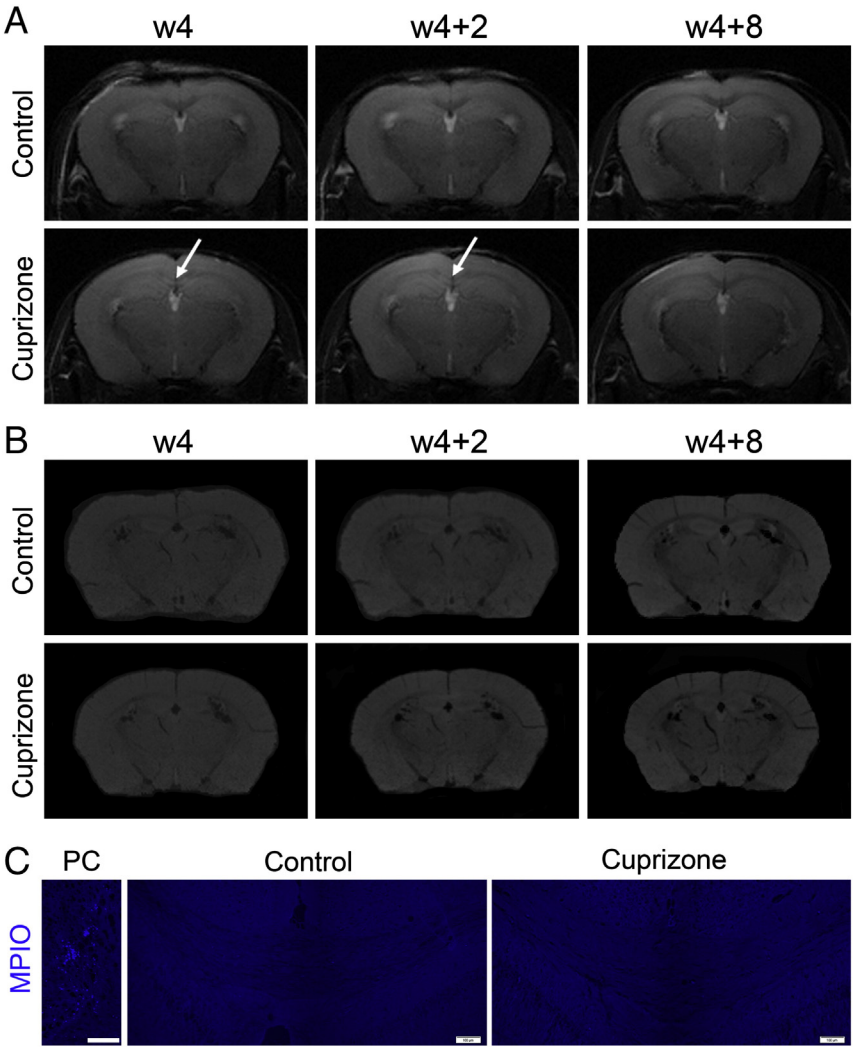

Fig. 4. MPIO-labeled SVZ NSPCs do not migrate towards the demyelinated splenium in the cuprizone mouse model. (A) Representative axial T_2-weighted images acquired *in vivo* at weeks 4, 6 and 12 p.i. (w4, w4 + 2 and w4 + 8). Images shown are from an age-matched control mouse injected with MPIOs in the lateral ventricle (Control, top row) and from a mouse that received a 4-week cuprizone treatment followed by 8 weeks of recovery on a regular rodent diet (Cuprizone, bottom row). Arrows point at hyper-intensity of the CC indicating demyelination/inflammation due to cuprizone administration. (B) Representative axial mIPs of 3D gradient-echo MR images acquired *in vivo* at weeks 4, 6 and 12 p.i. (w4, w4 + 2 and w4 + 8 respectively) indicate the absence of hypo-intense contrast at the level of the splenium of the CC. (C) Representative blue-fluorescence images taken at the level of the splenium of a mouse that received a 0.2% cuprizone diet for 4 weeks followed by 8 weeks of recovery on standard rodent chow (Cuprizone) and an age matched control mouse (Control, scale bar = 100 μm). A positive control (PC) of MPIOs near the injection tract is shown to illustrate how MPIOs can be identified in the CNS (scale bar = 200 μm).

(Fig. 5D). Statistical analysis revealed a significant increase of the BLI signal overtime ($p < 0.001$) for the cuprizone-treated group and the control group ($p = 0.049$). While no significant differences were found between the control group and the cuprizone-treated group at week 2 post-LVv injection ($p = 0.206$), a higher BLI signal was found in the cuprizone-treated group compared to the control group at week 12 post-LVv injection ($p = 0.002$). Moreover, the migration behavior of the cuprizone-treated group differs from the control group and this is reflected by a time and group interaction ($p = 0.001$). Finally, we performed histological quantification of the eGFP positive cells present in the OB at week 12 post-LVv injection in both the control and cuprizone-treated groups (Fig. 6A) and confirmed the higher number of LVv-labeled NSPCs arriving in the OB of cuprizone-treated mice as compared to control mice (Fig. 5E, $p = 0.026$). Furthermore, immunofluorescence staining for both groups confirmed that eGFP-labeled cells residing the OB co-localized with the neuronal marker NeuN, but not with IBA1 (microglia) or GFAP (astrocytes, Fig. 6B). In agreement with the higher BLI signal observed in the SVZ of cuprizone-treated mice as compared to control mice (see above, Fig. 5B), our results suggest an increased proliferation of NSPCs in the SVZ and eventually a higher number of NSPCs that migrate to the OB of cuprizone-treated mice.

Discussion

We investigated the contribution of endogenous SVZ NSPCs to the remyelination process in the cuprizone mouse model by means of MRI- and BLI-based *in vivo* longitudinal monitoring of SVZ NSPC migration. Using these techniques, our data suggest that the origin of cells responsible for remyelination of the CC in the cuprizone mouse model is not the SVZ NSPC compartment, despite preceding observations of SVZ cell proliferation and migration following cuprizone treatment. The exact origin of the progenitor cells responsible for remyelination in the cuprizone model thus needs to be further investigated.

Previously, it has been suggested that SVZ-derived NSPCs are involved in remyelination of the corpus callosum following cuprizone-induced demyelination (Chen et al., 2012; Kipp et al., 2009; Mason et al., 2000; Petratos et al., 2004). However, we questioned whether SVZ-derived progenitor cells really are the cell population responsible for the observed remyelination in the cuprizone model as: (i) these

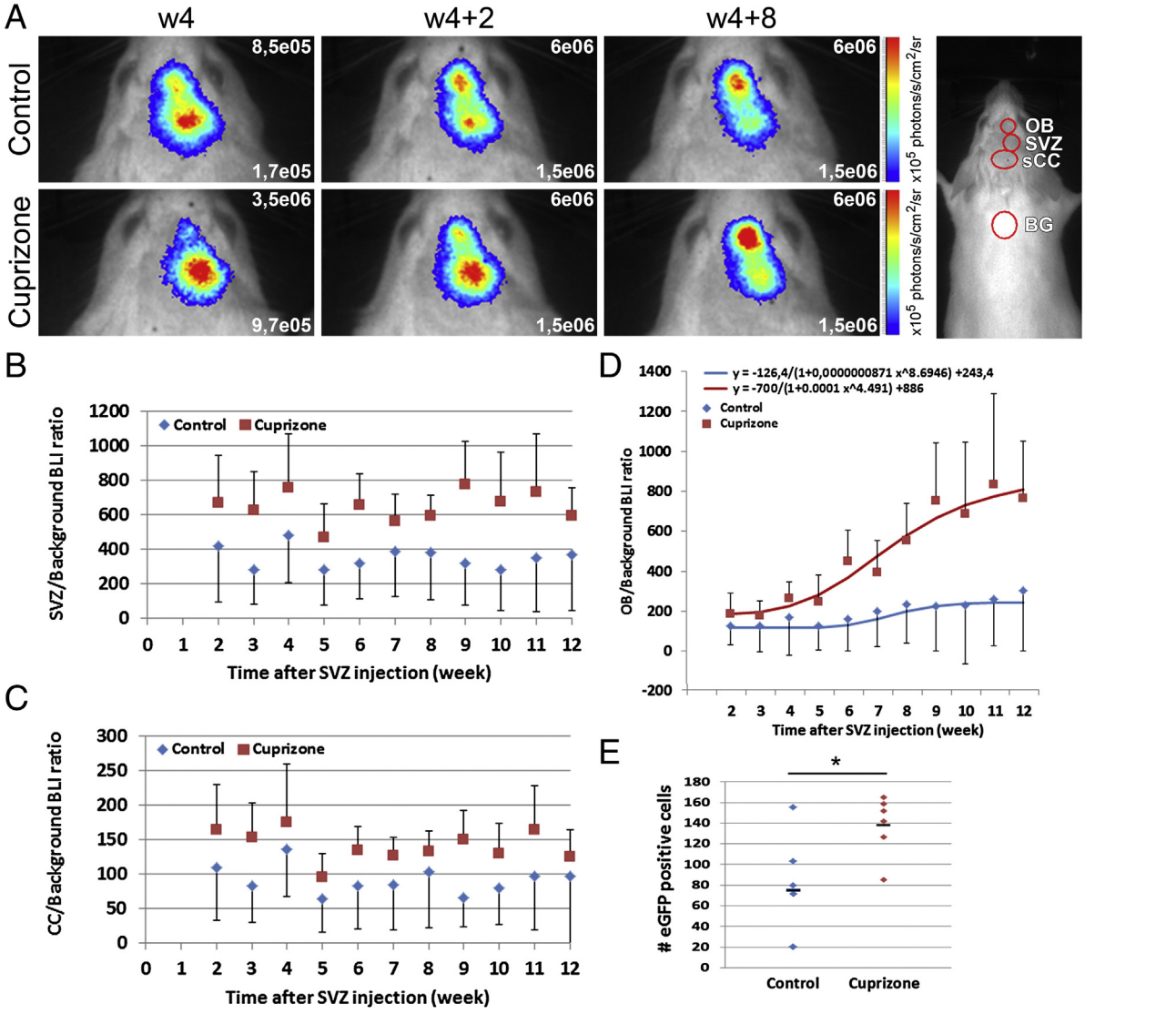

Fig. 5. LVv-labeled SVZ NSPCs do not migrate towards the demyelinated splenium but show an increased migration towards the OB in the cuprizone mouse model. (A) Representative BLI images of a mouse injected with the eGFP-fLuc encoding LVv and which received either a control diet for 12 weeks (Control) or a cuprizone diet for 4 weeks followed by 8 weeks recovery on standard rodent chow (Cuprizone). Images were acquired at 4, 6 and 12 weeks p.i. (w4, w4 + 2 and w4 + 8). The used ROI for the olfactory bulb (OB), subventricular zone (SVZ), splenium of the corpus callosum (sCC) and background (BG) is also shown. (B) The mean of the subventricular zone BLI signal ratio (BLI_{SVZ}/BLI_{BG}) during the 12 week period p.i. is shown for healthy control mice and for cuprizone treated mice (4 weeks of cuprizone diet followed by 8 weeks of recovery). (C) The mean of the sCC BLI signal ratio (BLI_{SCC}/BLI_{BG}) during the 12 week period p.i. is shown for healthy control mice and for cuprizone treated mice (4 weeks of cuprizone diet followed by 8 weeks of recovery). (D) The mean of the OB BLI signal ratio (BLI_{OB}/BLI_{BG}) during the 12 week period p.i. is shown for healthy control mice and for cuprizone treated mice (4 weeks of cuprizone diet followed by 8 weeks of recovery). Migration of fLuc labeled cells towards the OB can be appreciated by the sigmoidal distribution of the BLI signal over time. (E) Histological quantification of the number of eGFP positive cells found per low magnification picture of the OB for both healthy control mice (Control) and for cuprizone treated mice (4 weeks of cuprizone diet followed by 8 weeks of recovery (Cuprizone)). (*: p-value < 0.05).

earlier conclusions were drawn from histological studies, which do not allow to longitudinal follow-up the highly dynamic processes of cell proliferation, migration, differentiation and eventually remyelination, (ii) many $NG2^+$ OPCs are present throughout white and gray matter in the adult CNS and these are actively proliferating throughout adulthood (Dawson et al., 2003), and (iii) this widespread population of PDGFR-α/$NG2^+$ oligodendrocyte progenitor cells was shown to be able to differentiate into oligodendrocytes and Schwann cells in response to a demyelinating insult (Zawadzka et al., 2010). Therefore, in this study we investigated the involvement of SVZ-derived NSPCs during remyelination of the splenium following cuprizone treatment by means of MRI and BLI.

Additionally, we longitudinally investigated the constitutive migration of SVZ NSPCs towards the OB *in vivo*. While MRI analysis did not indicate significant differences between the healthy control group and the cuprizone-treated group, BLI analysis indicated a significant alteration of the SVZ NSPC migration from the SVZ to the OB in cuprizone-treated mice as compared to healthy control mice. Given the preceding observations that cuprizone-induced CNS inflammation induces cell proliferation in the SVZ at early stages post-administration (Mason et al., 2000; Silvestroff et al., 2010) and that CNS inflammation can promote endogenous neurogenesis (Gonzalez-Perez et al., 2012), it is not unlikely that the latter might have caused significant proliferation of non-transduced and LVv-transduced NSPCs in the SVZ, thereby potentially explaining the increased BLI signal and number of $eGFP^+$ neurons we observed in the OB of cuprizone-treated mice as compared to healthy control mice. These findings are supported by the study of Picard-Riera et al., who observed an increased migration of SVZ NSPCs towards the OB following EAE induction (Picard-Riera et al., 2002). In contrast to the results obtained using the BLI approach, we were unable to visualize a cuprizone-induced increase in SVZ NSPC migration towards the OB by means of MRI. However, the latter can be explained

Please cite this article as: Guglielmetti, C., et al., Multimodal imaging of subventricular zone neural stem/progenitor cells in the cuprizone mouse model reveals increased neurogenic potential ..., NeuroImage (2013), http://dx.doi.org/10.1016/j.neuroimage.2013.07.080

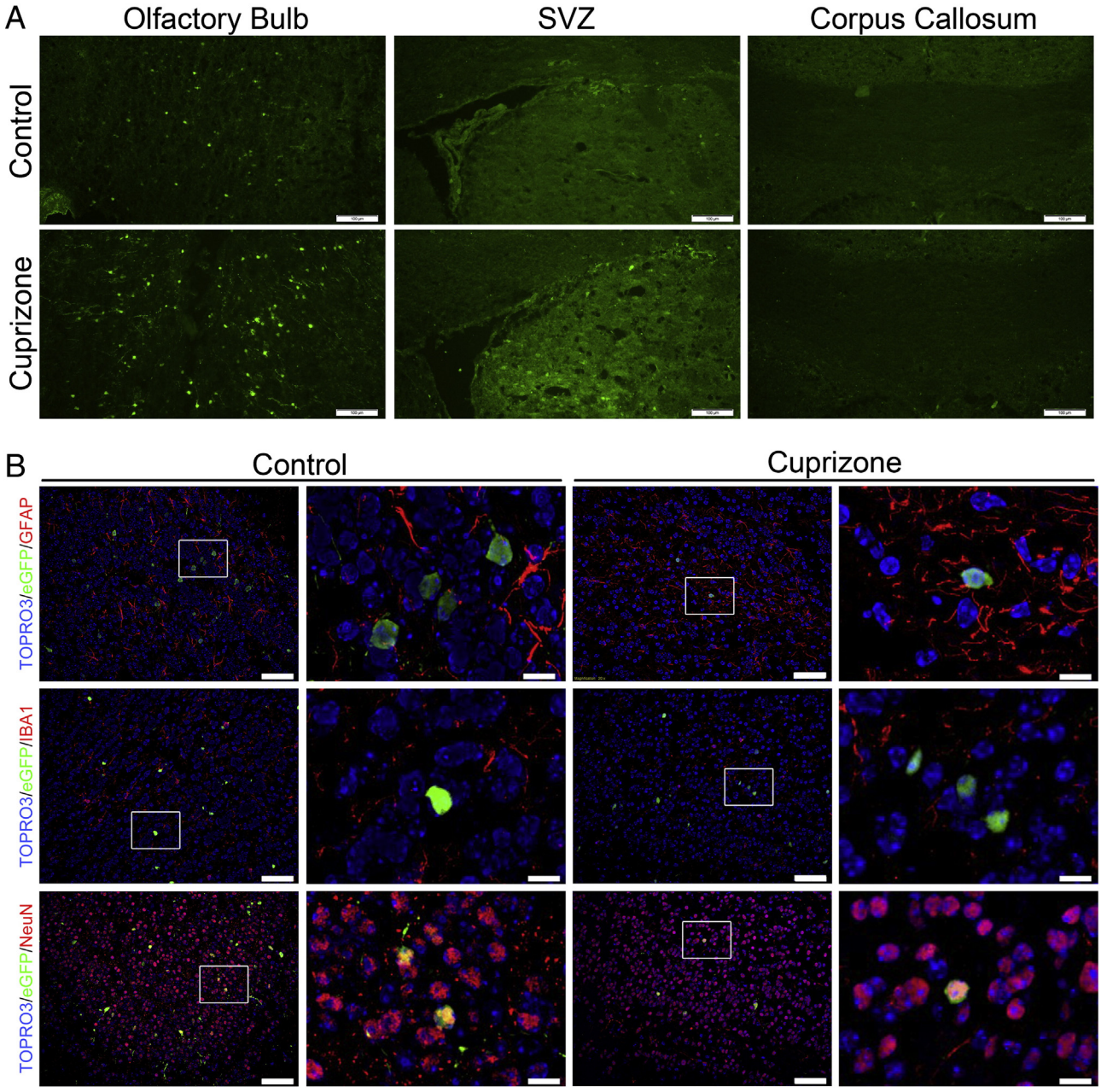

Fig. 6. Histological validation of LVv-labeled SVZ NSPC migration to the OB. (A) Representative histological images at 12 weeks following injection of an eGFP–fLuc encoding LVv in both control mice (Control) or mice fed a 0.2% cuprizone diet for 4 weeks followed by 8 weeks of recovery. eGFP positive cells can be observed in the olfactory bulb, the SVZ and parenchyma near the injection site (SVZ), but not in the splenium of the CC caudal to the injection site. (B) Representative histological images of the olfactory bulb at 12 weeks following injection of an eGFP–fLuc encoding LVv in both a control mouse (Control) or mice fed a 0.2% cuprizone diet for 4 weeks followed by 8 weeks of recovery. The left image shows a general overview of the olfactory bulb at a low magnification (scale bar = 50 μm) while the area inside the white rectangle is then shown at a higher magnification in the right image (scale bar = 10 μm). Cell nuclei were stained using TOPRO-3 and are shown in blue (false color), eGFP–fLuc transduced cells are shown by their green fluorescence and the corresponding cell-specific markers (IBA1, GFAP and NeuN) are shown in red (red fluorescence).

by the dilution of internalized MPIOs among daughter cells in the SVZ following cell proliferation (Walczak et al., 2007), which is in contrast with the LVv transduction approach where all progeny of initially transduced cells remains labeled.

While previous reports have described visualization of NSPC migration during the first days to weeks post-MPIO labeling, we only observed the start of migration at four weeks post-MPIO injection. However, several explanations can be suggested to explain this observation. First, Nieman et al. (2010) observed MPIO-labeled NSPC migration over the RMS already at 1 day post-injection. In contrast to our study, where MPIO were injected into the lateral ventricle, in their study MPIOs were directly injected into the SVZ, possibly transfecting also neuroblast committed NSPCs. Another possible explanation could be that MPIOs are injected too far to the back, which has been suggested to result in MPIO retention in the choroid plexus (Granot et al., 2011). However, although in our study we did occasionally observe MPIOs in the choroid plexus, most of the MPIOs were near the injection tract and within the ventricle wall of the SVZ. In addition, it is currently also well described that different MPIO coatings can influence NSPC MPIO uptake and therefore might influence MPIO-labeled NSPC migration (Tang and Shapiro, 2011; Vreys et al., 2010).

Finally, regarding both methods used for imaging SVZ NSPC migration, several differences can be noted between the two techniques. (i) In agreement with a previous observation by Nieman et al. (2010), in our study we also observed that around 30% of MPIOs in the OB collocate with IBA1$^+$ microglia, which is indicative of MPIO phagocytosis

Please cite this article as: Guglielmetti, C., et al., Multimodal imaging of subventricular zone neural stem/progenitor cells in the cuprizone mouse model reveals increased neurogenic potential ..., NeuroImage (2013), http://dx.doi.org/10.1016/j.neuroimage.2013.07.080

by microglia upon cell death of the originally labeled neuronal cell population. (ii) There is also a difference in cell labeling speed between the BLI and MRI approach. While following MPIO injection, a continuous labeling of NSPCs might occur during the whole experiment, LVv injection results of in an immediate (hours to days) transduction of SVZ NSPCs (Geraerts et al., 2006). For the latter it also has to be noted that, independent of the relatively fast transduction, stable expression of the introduced reporter genes is known to take up to 2 weeks (Baekelandt et al., 2002). Likewise, it would be interesting to study LVv-mediated transduction of SVZ NSPC with an MRI reporter gene, however this approach is currently suffering from low *in vivo* sensitivity (Vande Velde et al., 2011, 2012b).

Conclusions

In summary, we demonstrate using non-invasive imaging modalities – and confirm by histological analyses – that: (i) normal SVZ NSPC migration is altered following cuprizone treatment, and (ii) SVZ NSPCs do not seem to leave the RMS following cuprizone treatment and are therefore not responsible for the observed spontaneous remyelination of the splenium. Nevertheless, the fact that cuprizone-induced CNS inflammation and tissue damage is a trigger for increased migration of SVZ NSPC migration to the OB might open new directions for the identification of factors promoting OB neurogenesis. On the other hand, as inflammation induces proliferation of SVZ NSPC, one of the main challenges in the nearby future will be – if possible – to redirect their migration and or differentiation potential towards for example oligodendrocytes. However, future studies combining both longitudinal analyses with an in-depth histological characterization of SVZ NSPC fate will reveal if such a strategy is feasible to treat MS, or whether therapeutic intervention should explore other resident stem/progenitor populations.

Acknowledgments

We acknowledge the helpful assistance from Frank Rylant (Laboratory of Pathology, University of Antwerp) with histological techniques, David Berg with stereotactic injections (Bio-Imaging Lab, University of Antwerp) and Johan Van Audekerke for the technical MRI assistance (Bio-Imaging Lab, University of Antwerp). This work was in part supported by research grants from the European Union's Seventh Framework Programme (FP7/2007–2013) under grant agreement no. HEALTH-F2-2011-278850 (INMiND), and G.0136.11 and G.0130.11 (granted to AvDL and PP) of the Fund for Scientific Research-Flanders (FWO-Vlaanderen, Belgium). Nathalie De Vocht holds a PhD-studentship from the FWO-Vlaanderen. Caroline Guglielmetti is a holder of an IWT (Institute for the Promotion of Innovation through Science and Technology in Flanders (IWT-Vlaanderen)) PhD grant. Janaki Raman Rangarajan is funded in part by the IWT SBO project QUANTIVIAM (SBO-60819), KU Leuven Center of Excellence MoSAIC ("Molecular Small Animal Imaging Center") (KUL EF/05/08) and the KU Leuven program financing 'IMIR' (PF 10/017).

Conflict of interest

The authors declare no conflict of interest.

References

Baekelandt, V., Claeys, A., Eggermont, K., Lauwers, E., De Strooper, B., Nuttin, B., Debyser, Z., 2002. Characterization of lentiviral vector-mediated gene transfer in adult mouse brain. Hum. Gene Ther. 13, 841–853.

Barkhof, F., Bruck, W., De Groot, C.J., Bergers, E., Hulshof, S., Geurts, J., Polman, C.H., van der Valk, P., 2003. Remyelinated lesions in multiple sclerosis: magnetic resonance image appearance. Arch. Neurol. 60, 1073–1081.

Chen, L.P., Li, Z.F., Ping, M., Li, R., Liu, J., Xie, X.H., Song, X.J., Guo, L., 2012. Regulation of Olig2 during astroglial differentiation in the subventricular zone of a cuprizone-induced demyelination mouse model. Neuroscience 221, 96–107.

Couillard-Despres, S., Aigner, L., 2011. In vivo imaging of adult neurogenesis. Eur. J. Neurosci. 33, 1037–1044.

Couillard-Despres, S., Vreys, R., Aigner, L., Van der Linden, A., 2011. In vivo monitoring of adult neurogenesis in health and disease. Front. Neurosci. 5, 67.

Dawson, M.R., Polito, A., Levine, J.M., Reynolds, R., 2003. NG2-expressing glial progenitor cells: an abundant and widespread population of cycling cells in the adult rat CNS. Mol. Cell. Neurosci. 24, 476–488.

Doetsch, F., Caille, I., Lim, D.A., Garcia-Verdugo, J.M., Alvarez-Buylla, A., 1999. Subventricular zone astrocytes are neural stem cells in the adult mammalian brain. Cell 97, 703–716.

Franklin, R.J., Ffrench-Constant, C., 2008. Remyelination in the CNS: from biology to therapy. Nat. Rev. Neurosci. 9, 839–855.

Geraerts, M., Eggermont, K., Hernandez-Acosta, P., Garcia-Verdugo, J.M., Baekelandt, V., Debyser, Z., 2006. Lentiviral vectors mediate efficient and stable gene transfer in adult neural stem cells in vivo. Hum. Gene Ther. 17, 635–650.

Gonzalez-Perez, O., Gutierrez-Fernandez, F., Lopez-Virgen, V., Collas-Aguilar, J., Quinones-Hinojosa, A., Garcia-Verdugo, J.M., 2012. Immunological regulation of neurogenic niches in the adult brain. Neuroscience 226, 270–281.

Granot, D., Scheinost, D., Markakis, E.A., Papademetris, X., Shapiro, E.M., 2011. Serial monitoring of endogenous neuroblast migration by cellular MRI. NeuroImage 57, 817–824.

Kipp, M., Clarner, T., Dang, J., Copray, S., Beyer, C., 2009. The cuprizone animal model: new insights into an old story. Acta Neuropathol. 118, 723–736.

Likar, B., Viergever, M.A., Pernus, F., 2001. Retrospective correction of MR intensity inhomogeneity by information minimization. IEEE Trans. Med. Imaging 20, 1398–1410.

MacKenzie-Graham, A., Lee, E.F., Dinov, I.D., Bota, M., Shattuck, D.W., Ruffins, S., Yuan, H., Konstantinidis, F., Pitiot, A., Ding, Y., Hu, G., Jacobs, R.E., Toga, A.W., 2004. A multimodal, multidimensional atlas of the C57BL/6J mouse brain. J. Anat. 204, 93–102.

Maes, F., Collignon, A., Vandermeulen, D., Marchal, G., Suetens, P., 1997. Multimodality image registration by maximization of mutual information. IEEE Trans. Med. Imaging 16, 187–198.

Mason, J.L., Jones, J.J., Taniike, M., Morell, P., Suzuki, K., Matsushima, G.K., 2000. Mature oligodendrocyte apoptosis precedes IGF-1 production and oligodendrocyte progenitor accumulation and differentiation during demyelination/remyelination. J. Neurosci. Res. 61, 251–262.

Meier, D.S., Guttmann, C.R.G., 2003. Time-series analysis of MRI intensity patterns in multiple sclerosis. NeuroImage 20, 1193–1209.

Menn, B., Garcia-Verdugo, J.M., Yaschine, C., Gonzalez-Perez, O., Rowitch, D., Alvarez-Buylla, A., 2006. Origin of oligodendrocytes in the subventricular zone of the adult brain. J. Neurosci. 26, 7907–7918.

Nieman, B.J., Shyu, J.Y., Rodriguez, J.J., Garcia, A.D., Joyner, A.L., Turnbull, D.H., 2010. In vivo MRI of neural cell migration dynamics in the mouse brain. NeuroImage 50, 456–464.

Panizzo, R.A., Kyrtatos, P.G., Price, A.N., Gadian, D.G., Ferretti, P., Lythgoe, M.F., 2009. In vivo magnetic resonance imaging of endogenous neuroblasts labelled with a ferumoxide–polycation complex. NeuroImage 44, 1239–1246.

Petratos, S., Gonzales, M.F., Azari, M.F., Marriott, M., Minichiello, R.A., Shipham, K.A., Profyris, C., Nicolaou, A., Boyle, K., Cheema, S.S., Kilpatrick, T.J., 2004. Expression of the low-affinity neurotrophin receptor, p75(NTR), is upregulated by oligodendroglial progenitors adjacent to the subventricular zone in response to demyelination. Glia 48, 64–75.

Picard-Riera, N., Decker, L., Delarasse, C., Goude, K., Nait-Oumesmar, B., Liblau, R., Pham-Dinh, D., Evercooren, A.B., 2002. Experimental autoimmune encephalomyelitis mobilizes neural progenitors from the subventricular zone to undergo oligodendrogenesis in adult mice. Proc. Natl. Acad. Sci. U. S. A. 99, 13211–13216.

Praet, J., Reekmans, K., Lin, D., De Vocht, N., Bergwerf, I., Tambuyzer, B., Daans, J., Hens, N., Goossens, H., Pauwels, P., Berneman, Z., Van der Linden, A., Ponsaerts, P., 2012. Cell type-associated differences in migration, survival and immunogenicity following grafting in CNS tissue. Cell Transplant. 21, 1867–1881.

Reekmans, K.P., Praet, J., De Vocht, N., Tambuyzer, B.R., Bergwerf, I., Daans, J., Baekelandt, V., Vanhoutte, G., Goossens, H., Jorens, P.G., Ysebaert, D.K., Chatterjee, S., Pauwels, P., Van Marck, E., Berneman, Z.N., Van der Linden, A., Ponsaerts, P., 2011. Clinical potential of intravenous neural stem cell delivery for treatment of neuroinflammatory disease in mice? Cell Transplant. 20, 851–869.

Reumers, V., Deroose, C.M., Krylyshkina, O., Nuyts, J., Geraerts, M., Mortelmans, L., Gijsbers, R., Van den Haute, C., Debyser, Z., Baekelandt, V., 2008. Noninvasive and quantitative monitoring of adult neuronal stem cell migration in mouse brain using bioluminescence imaging. Stem Cells 26, 2382–2390.

Shapiro, E.M., Gonzalez-Perez, O., Manuel Garcia-Verdugo, J., Alvarez-Buylla, A., Koretsky, A.P., 2006. Magnetic resonance imaging of the migration of neuronal precursors generated in the adult rodent brain. NeuroImage 32, 1150–1157.

Silvestroff, L., Bartucci, S., Soto, E., Gallo, V., Pasquini, J., Franco, P., 2010. Cuprizone-induced demyelination in CNP::GFP transgenic mice. J. Comp. Neurol. 518, 2261–2283.

Skripuletz, T., Gudi, V., Hackstette, D., Stangel, M., 2011. De- and remyelination in the CNS white and grey matter induced by cuprizone: the old, the new, and the unexpected. Histol. Histopathol. 26, 1585–1597.

Sumner, J.P., Shapiro, E.M., Maric, D., Conroy, R., Koretsky, A.P., 2009. In vivo labeling of adult neural progenitors for MRI with micron sized particles of iron oxide: quantification of labeled cell phenotype. NeuroImage 44, 671–678.

Tang, K.S., Shapiro, E.M., 2011. Enhanced magnetic cell labeling efficiency using $-NH_2$ coated MPIOs. Magn. Reson. Med. 65, 1564–1569.

Vande Velde, G., Rangarajan, J.R., Toelen, J., Dresselaers, T., Ibrahimi, A., Krylychkina, O., Vreys, R., Van der Linden, A., Maes, F., Debyser, Z., Himmelreich, U., Baekelandt, V., 2011. Evaluation of the specificity and sensitivity of ferritin as an MRI reporter gene in the mouse brain using lentiviral and adeno-associated viral vectors. Gene Ther. 18, 594–605.

Vande Velde, G., Couillard-Despres, S., Aigner, L., Himmelreich, U., van der Linden, A., 2012a. In situ labeling and imaging of endogenous neural stem cell proliferation and migration. Wiley Interdiscip. Rev. Nanomed. Nanobiotechnol. 4, 663–679.

Please cite this article as: Guglielmetti, C., et al., Multimodal imaging of subventricular zone neural stem/progenitor cells in the cuprizone mouse model reveals increased neurogenic potential ..., NeuroImage (2013), http://dx.doi.org/10.1016/j.neuroimage.2013.07.080

Vande Velde, G., Raman Rangarajan, J., Vreys, R., Guglielmetti, C., Dresselaers, T., Verhoye, M., Van der Linden, A., Debyser, Z., Baekelandt, V., Maes, F., Himmelreich, U., 2012b. Quantitative evaluation of MRI-based tracking of ferritin-labeled endogenous neural stem cell progeny in rodent brain. NeuroImage 62, 367–380.

Vreys, R., Vande Velde, G., Krylychkina, O., Vellema, M., Verhoye, M., Timmermans, J.P., Baekelandt, V., Van der Linden, A., 2010. MRI visualization of endogenous neural progenitor cell migration along the RMS in the adult mouse brain: validation of various MPIO labeling strategies. NeuroImage 49, 2094–2103.

Walczak, P., Kedziorek, D.A., Gilad, A.A., Barnett, B.P., Bulte, J.W., 2007. Applicability and limitations of MR tracking of neural stem cells with asymmetric cell division and rapid turnover: the case of the shiverer dysmyelinated mouse brain. Magn. Reson. Med. 58, 261–269.

Yang, J., Liu, J., Niu, G., Chan, K.C., Wang, R., Liu, Y., Wu, E.X., 2009. In vivo MRI of endogenous stem/progenitor cell migration from subventricular zone in normal and injured developing brains. NeuroImage 48, 319–328.

Zawadzka, M., Rivers, L.E., Fancy, S.P., Zhao, C., Tripathi, R., Jamen, F., Young, K., Goncharevich, A., Pohl, H., Rizzi, M., Rowitch, D.H., Kessaris, N., Suter, U., Richardson, W.D., Franklin, R.J., 2010. CNS-resident glial progenitor/stem cells produce Schwann cells as well as oligodendrocytes during repair of CNS demyelination. Cell Stem Cell 6, 578–590.

Please cite this article as: Guglielmetti, C., et al., Multimodal imaging of subventricular zone neural stem/progenitor cells in the cuprizone mouse model reveals increased neurogenic potential ..., NeuroImage (2013), http://dx.doi.org/10.1016/j.neuroimage.2013.07.080